IEEE Access
Multidisciplinary | Rapid Review | Open Access Journal

Received 9 January 2024, accepted 8 February 2024, date of publication 21 February 2024, date of current version 29 February 2024.

Digital Object Identifier 10.1109/ACCESS.2024.3368858

APPLIED RESEARCH

Full-Wave Digital Predistortion Linearization Based on Memory Polynomials for HF Power Amplifiers

JUNSHI LV[1], (Student Member, IEEE), GAOMING XU[1], CHENGTING ZHANG[2], HAILI ZHANG[1], AND TAIJUN LIU[1], (Senior Member, IEEE)
[1]Faculty of Electrical Engineering and Computer Science, Ningbo University, Ningbo, Zhejiang 315211, China
[2]China Tobacco Zhejiang Industrial Company Ltd., Ningbo 315504, China

Corresponding author: Taijun Liu (liutaijun@nbu.edu.cn)

This work was supported in part by the National Natural Science Foundation of China under Grant 62371266, Grant U1809203, and Grant 62071264; and in part by the Key Research Project from China Tobacco Zhejiang Industrial Company Ltd., under Grant H2023000125.

ABSTRACT In order to suppress the intermodulation distortion and harmonic distortion caused by the nonlinearity of a HF power amplifier (PA), this paper presents a nonlinear correction method for full wave digital predistortion (DPD) of a HF PA based on a memory polynomial. First, the required full wave nonlinear signal is obtained by using the negative feedback iteration method for the digital predistorter, and then a full wave signal including the fundamental wave, each order harmonics and all intermodulation signals is constructed using the memory polynomial. Finally, the full wave memory polynomial model is constructed by shifting the spectrum of the same order connected harmonics and their adjacent intermodulation components. To verify the correctness of the method, the algorithm is simulated first, and then an actual PA is used to verify the experiment. A 5W short-wave PA is used to test and verify dual-tone signals at different carrier frequencies. The experimental results show that after linearization of full-wave DPD, the second and third harmonic components are improved by more than 35 dB, and the intermodulation distortion is improved by at least 9 dB, which effectively suppresses the intermodulation distortion and harmonic distortion.

INDEX TERMS Digital predistortion (DPD), full wave memory polynomial (FWMP), harmonic suppression, linearization, spectrum shifting.

I. INTRODUCTION

Shortwave communication has always been an important means of wireless communication, especially for emergency communication, aviation communication and navigation, military communication and other application scenarios, due to its unique advantages such as a long transmission distance and no dependence on ground base stations. For short-wave communication systems, the fundamental signal amplified by the short-wave power amplifier (PA) produces serious inter-harmonic distortion due to the non-linearity of the PA. Intermodulation distortion is commonly compensated for by employing baseband digital predistortion (DPD) technology [1], [2], [3], [4], [5], while harmonic and higher-order intermodulation distortion signals are typically subjected to filtering or suppression. However, due to the wide frequency range of 1.6MHz to 30MHz in shortwave communication systems, a single filter, as depicted in Figure 1, is insufficient for achieving harmonic suppression across the entire shortwave band. Therefore, it becomes necessary to employ a bulky filter bank comprising up to seven filters that cover different frequency ranges. Consequently, this not only results in the proliferation of large-sized shortwave radio stations but also significantly amplifies system complexity. Therefore, the suppression of harmonic and high-order intermodulation distortion generated by PA to eliminate or simplify the filter group has always been a pivotal technical challenge encountered in shortwave communication. Particularly in recent years, with the emergence of applications such as drones, there is an urgent demand for miniaturization and lightweight

The associate editor coordinating the review of this manuscript and approving it for publication was Pedro Miguel Cabral.

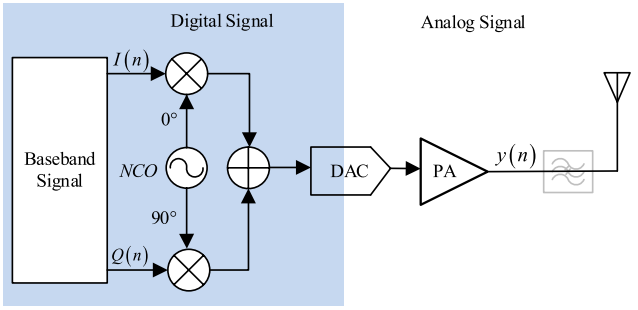

FIGURE 1. Block diagram of a traditional communication system.

design of shortwave communication systems. Consequently, it has become imperative to employ advanced digital techniques to address this issue.

In order to remove the complex short-wave filter banks, Kashchenko [6] proposed a harmonic injection method, which involves introducing a harmonic injection channel in the high-frequency path to compensate for harmonic distortion across the entire output frequency range. The present work by Pazhouhesh and Kitchen [7] presents a novel approach for enhancing the efficiency of a wideband AB class push-pull PA with second harmonic injection, achieved through injecting the second harmonic via the center tap of a uniform harmonic trap, thereby extending its frequency bandwidth. Wang et al. [8] proposed a methodology to investigate the trade-off between power efficiency of PA and the corresponding complexity of digital pre-distortion models required for linearization. Singhal and Rawat [9] proposed a transmitter structure without filters, incorporating digital-assisted harmonic cancellation by employing neural networks to accurately model harmonics and intermodulation distortion. Cho et al. [10] proposed a multi-stage predistortion linearization circuit that ingeniously integrates second harmonic and difference frequency techniques. The HTBP model, proposed by Chen et al. [11] and Xu et al. [12], is based on the Hilbert transform technique. This model applies the Hilbert transform to the fundamental wave signal and utilizes harmonic polynomials to accurately represent intermodulation distortion and harmonic distortion. The harmonic cancellation memory polynomial (HCMP) model, proposed by Ren et al. [13], is derived from the basis of MP and exhibits significant advancements in the mitigation of second and third harmonic distortions. The harmonic cancellation-decomposed vector rotation (HC-DVR) model, proposed by Liu [14], enhances the harmonic cancellation performance based on the decomposed vector rotation (DVR) model.

The aforementioned method exhibits a favorable suppression effect on harmonic and higher-order intermodulation distortion signals; However, there still exists a notable residual of such distortions. Further optimization and refinement are imperative to enhance the efficacy of DPD methods in attenuating harmonic and higher-order intermodulation distortion signals. The present article proposes a novel full-wave DPD model based on memory polynomials, thereby enhancing the fitting accuracy of the model for harmonic and intermodulation distortion signals through refinement of higher-order terms within the memory polynomial. By effectively compensating for intermodulation distortion, this approach achieves superior precision in suppressing harmonic distortion.

The rest of the paper is organized as follows: The second part provides a comprehensive analysis of the generation method for complex fundamental wave signals, along with harmonic and higher-order intermodulation distortion signals. It explores the correlation between traditional memory polynomials and harmonic and intermodulation distortion signals, proposes a frequency spectrum shifting approach for harmonic and higher-order intermodulation distortion signals, and elucidates the characteristics of full-wave memory polynomials (FWMP). Additionally, the algorithm's theoretical derivation is presented. The third section presents the digital simulation and experimental verification results of full-wave DPD utilizing memory polynomials. Finally, a comprehensive summary is provided for the experimental findings and the entire paper.

II. FULL WAVE DPD METHOD BASED ON MEMORY POLYNOMIAL

DPD linearization is commonly employed in the baseband or intermediate frequency domain to preprocess signals using a digital predistorter, prior to up-conversion to radio frequency (RF), for mitigating intermodulation components induced by inherent nonlinearity of RF PA. In order to effectively suppress the fundamental-wave's various harmonic components, and their adjacent intermodulation components generated by the nonlinearity of the PA and its neighboring intermodulation components, it is necessary to perform predistortion linearization processing on the modulated RF signal (fundamental wave signal). This distinguishes from traditional DPD techniques that primarily compensate for intermodulation components near the fundamental wave, as full-wave DPD performed on the RF channel can suppress various intermodulation components along with harmonic components. The term 'full-wave' refers to digitally linearizing not only the fundamental wave signal and its harmonics but also intermodulation signals near both fundamental and harmonic frequencies.

The schematic diagram in Figure 2 illustrates the fundamental principle of a full-wave DPD system. To extract predistorter parameters and obtain the desired signal, an iterative application of negative feedback to the PA's feedback signal is necessary [10]. The principle of the negative feedback iterative method is shown in formula (1).

$$x_k\,(n) = x_{k-1}\,(n) + w_0\,(u\,(n) - \lambda \tilde{y}_k\,(n)) \tag{1}$$

where $x_k\,(n)$ and $\tilde{y}_k\,(n)$ denote the normalized input and output of PA in the k-th iteration, and $u\,(n)$ is the original input signal here is fundamental wave. λ denotes the feedback depth, and w_0 is a control factor used to adjust the

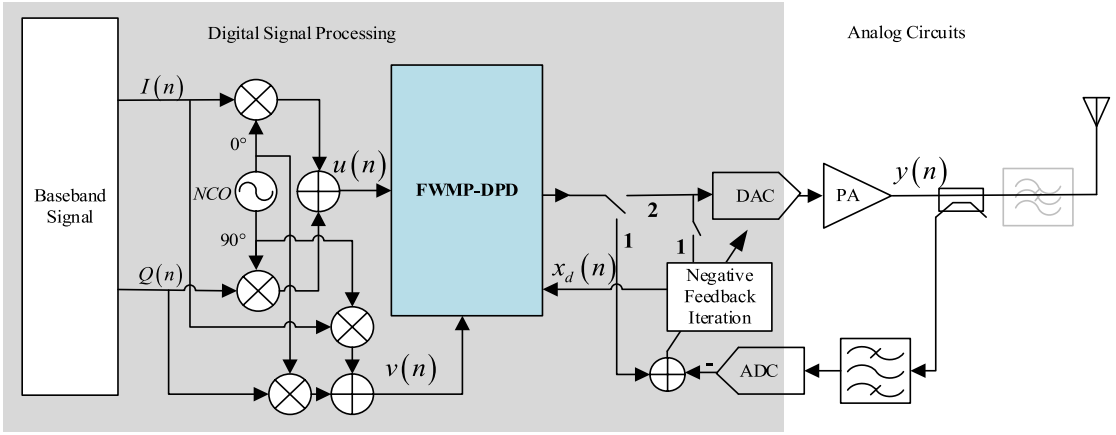

FIGURE 2. Full wave DPD system block diagram.

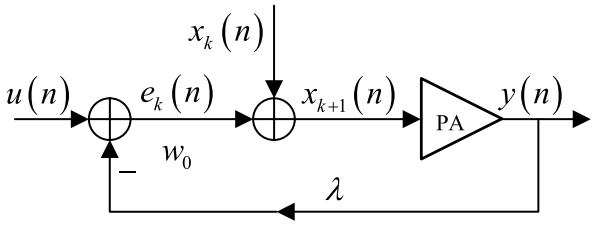

FIGURE 3. The flowchart of the negative feedback iteration.

convergence of negative feedback iteration. In [16] and [17] λ can be seen as the average power gain. In [11], λ and w_0 were carefully chosen to be 1 and 0.6, respectively. It should be pointed out that when we use the negative feedback iteration method, the system cannot be pre-distorted it works for offline training, as shown in Figure 2, the switch can only be in position 1 or position 2. Negative feedback iteration can be regarded as a training mode of DPD. Figure 4 shows a flowchart that explains the negative feedback iteration scheme in detail.

A. NONLINEARITY ANALYSIS OF HIGHER-ORDER TERMS OF POLYNOMIALS

The conventional memory polynomial, as depicted in equation (2), is specifically tailored for baseband signals and lacks the capability to accurately represent harmonic and adjacent intermodulation signal components. The utilization of the memory polynomial expressed by equation (3) is imperative when dealing with full-wave signals that encompass fundamental, harmonic, and intermodulation components. In formulas (2) and (3), k is the polynomial order, q is the memory depth, and c_{kq} is the undetermined model parameter. The x (n) in (2) refers to the baseband complex signal, and the x (n) in (3) refers to the fundamental real signal which is baseband signal modulated signal after digital

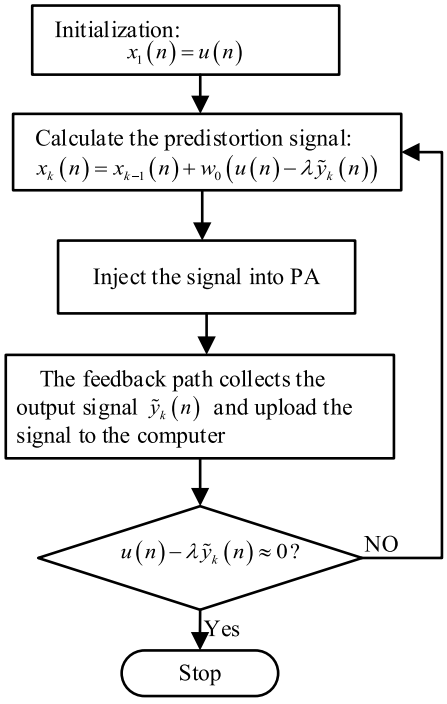

FIGURE 4. Comparison of the initial phase of monophonic.

up-conversion.

$$y(n) = \sum_{q=0}^{M-1} \sum_{k=1}^{K} c_{kq} x(n-q) |x(n-q)|^{k-1} \quad (2)$$

$$y(n) = \sum_{q=0}^{M-1} \sum_{k=1}^{K} c_{kq} x^{k}(n-q) \quad (3)$$

Due to the fact that the fundamental wave signal is a purely real signal without any imaginary component, it not only generates harmonics of the same order and intermodulation components in close proximity to these harmonics,

but also gives rise to numerous lower-order harmonics and intermodulation components surrounding these harmonics. Consequently, this intricate phenomenon adds complexity to the comprehensive analysis. Therefore, we will initially examine the relationship between the fundamental wave and harmonics. Taking a single-tone signal with an angular frequency ω, initial phase φ, and signal amplitude A as an example using formula (4), it is important to note that the second harmonic component of the fundamental wave signal x (n) is not solely generated by x^2 (n), but also by higher-order even terms such as x^4 (n), x^6 (n), etc., as demonstrated in formulas (5)-(7). This is also a significant contributing factor to the suboptimal full-wave predistortion effects observed in traditional polynomial fitting methods.

$$x\,(n) = A\cos\left(\omega n T_s + \varphi\right) \tag{4}$$

$$x^2\,(n) = \frac{1}{2}A\cos\left(2\omega n T_s + 2\varphi\right) + \frac{1}{2}A \tag{5}$$

$$x^4\,(n) = \frac{1}{8}A\cos\left(4\omega n T_s + 4\varphi\right) + \frac{1}{2}A\cos\left(2\omega n T_s + 2\varphi\right) + \frac{3}{8}A \tag{6}$$

$$x^6\,(n) = \frac{1}{32}A\cos\left(6\omega n T_s + 6\varphi\right) + \frac{3}{16}A\cos\left(4\omega n T_s + 4\varphi\right) + \frac{15}{32}A\cos\left(2\omega n T_s + 2\varphi\right) + \frac{5}{16}A \tag{7}$$

The fundamental signal and its harmonic signals exhibit the following characteristics:

1) In a full-wave signal, the initial phase of harmonics is an integer multiple of the initial phase of the fundamental wave. Theoretically, the initial phase of the second harmonic is twice that of the fundamental wave, while for higher-order harmonics such as the third harmonic, their initial phases are proportional to their respective harmonic numbers in relation to the fundamental wave.

2) The phases of harmonics of different orders may not necessarily be identical. In theory, adjacent harmonics exhibit distinct initial phases when $\varphi \neq 0$.

3) The lower-order harmonic components generated by higher-order terms of the fundamental signal are not necessarily smaller than those generated by lower-order terms at the same order. Generally, the same-order harmonic components produced by higher-order terms tend to be smaller in magnitude compared to those produced by lower-order terms.

At $\varphi = \pi/2$, during the first half cycle of x (n), the fundamental wave and the second and fourth harmonic waves demonstrate contrasting trends. Conversely, in the second half cycle of x (n), these waves exhibit similar trends, as depicted in Figure 5. Diverse initial phase of the fundamental wave results in distinct harmonic characteristics. Constructing a predistorter necessitates not only fitting the amplitude of the full-wave signal but also aligning its phase characteristics. As PA operate in the real domain, they inherently introduce phase distortion. When harmonic phases are not multiples of the fundamental phase, fitting becomes challenging. Complexifying the fundamental signal offers a clear advantage in adjusting the phase and enables better fitting of the PA's full-wave characteristics. This allows for construction of a full-wave predistortion linearizer based on this approach.

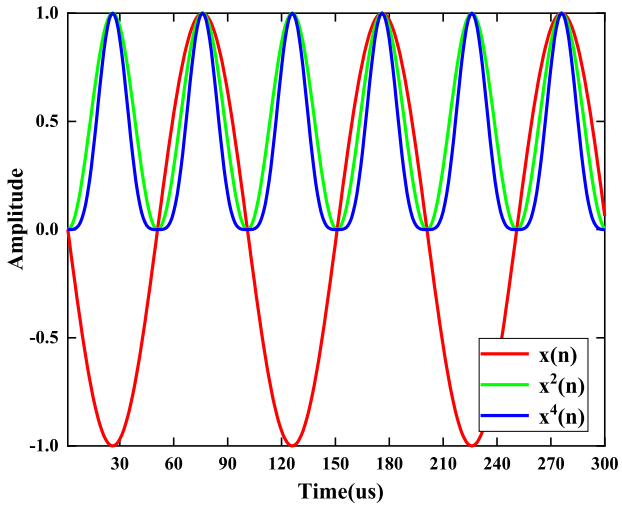

FIGURE 5. The negative feedback loop for iteration.

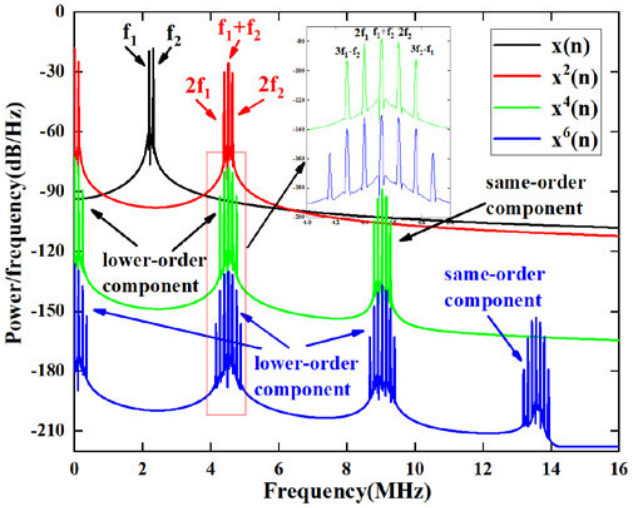

FIGURE 6. Spectrum analysis of the higher-order terms of the fundamental waves for dual-tone signals.

The relationship between the fundamental wave and intermodulation components is subsequently examined. When the fundamental signal comprises dual-tone or multi-tone signals, the nonlinearity of the PA not only gives rise to harmonic components but also engenders intermodulation components. To avoid excessive verbosity while effectively illustrating this issue, simulated spectral results of the fundamental wave signal, along with its second, fourth, and sixth-order are employed as exemplars for analysis. Due to the inherent symmetry between positive and negative frequencies, Figure 6 illustrates the positive frequency component. The coefficients

of x^2 (n), x^4 (n), and x^6 (n) are uniformly set to 1. To facilitate comparison, a downward shift of 50 dB and 100 dB has been applied to x^4 (n) and x^6 (n) respectively. As depicted in Figure 6, it is evident that x^6 (n) exhibits a spectrum comprising of a direct current component (zero frequency), the fundamental wave, harmonics, and intermodulation components around both the fundamental wave and each harmonic.

Considering the characteristics of PA's harmonics and intermodulation components discussed earlier, if our objective is to solely suppress the second harmonic of the PA's output along with its adjacent intermodulation components, it becomes imperative not only to modify x^2 (n), but also x^4 (n), x^6 (n), and even higher even power terms. However, altering x^4 (n) and x^6 (n) would inevitably lead to modifications in other associated components such as fourth harmonics, sixth harmonics, related sum-frequency components, and difference frequency components. This observation highlights that the model presented in equation (2) oversimplifies the accurate representation of amplifier harmonics and intermodulation characteristics.

B. GENERATING HARMONIC AT THE SAME ORDER AS HIGHER-ORDER TERMS AND INCORPORATING SUM-FREQUENCY COMPONENTS WITHIN HARMONIC

The electromagnetic field serves as the medium for signal propagation, which can be mathematically expressed using complex numbers. A single tone signal with angular frequency ω and amplitude A (t) can be represented by formula (8), where its real part is cos (ωt), its imaginary part is sin (ωt), and i denotes the imaginary unit.

$$A(t)\, e^{i\omega t} = A(t)\, cos(\omega t) + iA(t)\, sin(\omega t) \tag{8}$$

The NTH harmonic can be represented by formula (9), where n is a positive integer, in accordance with the expression provided. When $n = 1$, it corresponds to the fundamental wave; when $n = 2$, it represents the second harmonic; and when $n = 3$, it signifies the third harmonic, continuing in this manner.

$$A(t)\, e^{in\omega t} = A(t)\, cos(n\omega t) + iA(t)\, sin(n\omega t) \tag{9}$$

The baseband modulated signal is assumed to have an angular frequency of ω_b and an amplitude of A (t), while the carrier signal (i.e., the fundamental wave) has an angular frequency of ω_{up}. Upon quadratic modulation of the baseband signal onto the carrier, a complex form of the fundamental signal (referred to as the fundamental complex signal) is obtained, as shown in equation (10). The first bracket represents the real part of the fundamental complex signal, which corresponds to the fundamental signal denoted as u (n). The second bracket encompasses the imaginary component of the primary complex signal, which is derived by multiplying the real component of the baseband signal with the imaginary part of NCO and also by multiplying the imaginary part of the baseband signal with the real part of NCO, denoted as v (n). The basic complex signal can be represented by formula (11) accordingly. It is worth noting that the fundamental signal

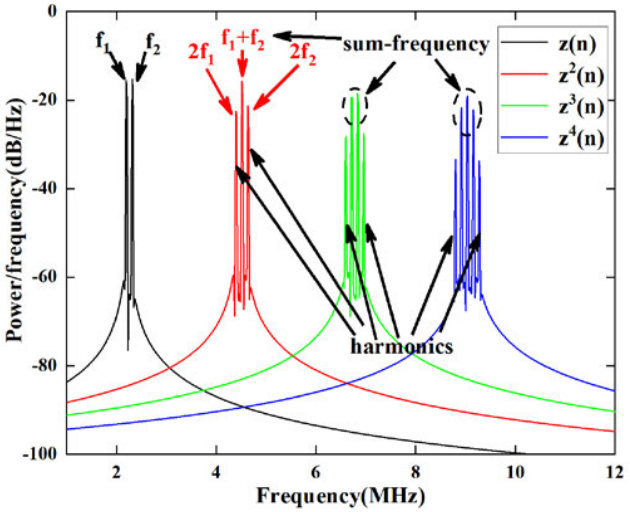

FIGURE 7. Analysis the higher-order of fundamental complex signal for dual-tone signals.

can also yield the basic complex signal through Hilbert transform [8], [9]. Unlike the Hilbert transform, which requires convolution of the fundamental signal, our approach in this paper solely relies on multiplication and addition operations, offering a more convenient implementation.

$$\begin{aligned} z &= A(t)\, e^{i\omega_b t}\, e^{i\omega_{up} t} \\ &= A(t)\, (\cos(\omega_b t) + i \sin(\omega_b t))\, (\cos(\omega_{up} t) + i \sin(\omega_{up} t)) \\ &= A(t)\, \{\cos(\omega_b t) \cos(\omega_{up} t) - \sin(\omega_b t) \sin(\omega_{up} t)\} \\ &\quad + iA(t)\, \{\sin(\omega_b t) \cos(\omega_{up} t) + \cos(\omega_b t) \sin(\omega_{up} t)\} \end{aligned} \tag{10}$$

$$z(n) = A(t)\, u(n) + iA(t)\, v(n) \tag{11}$$

From a spectral analysis perspective, the higher-order terms of a complexified fundamental signal exclusively comprise harmonics, parasitic and intermodulation components within the harmonic frequencies, while excluding lower-order harmonic components, adjacent beat or sum-frequency components, as well as DC components. For instance, considering a dual-tone signal characterized by angular frequencies ω_1 and ω_2, an initial phase φ of 0, and an amplitude of 1, the complex representation of the fundamental wave can be described using equations (12)-(14). The corresponding spectrum is depicted in Figure 7. The term z^4 (n) denotes the fourth harmonic along with its associated sum-frequency components within the harmonics. Notably, there are no lower harmonics or related components present; instead, the sum-frequency components within the harmonics surpass the harmonic components themselves. The modification of the higher-order terms in the pluralized fundamental signal has no impact on other lower-order terms, thereby enabling optimization of the model structure.

$$\begin{aligned} z^2(n) &= \left(A_1(t)\, e^{i\omega_1 n T_s} + A_2(t)\, e^{i\omega_2 n T_s}\right)^2 \\ &= A_1^2(t)\, e^{i2\omega_1 n T_s} + A_2^2(t)\, e^{i2\omega_2 n T_s} \\ &\quad + 2A_1(t) A_2(t)\, e^{i(\omega_1+\omega_2) n T_s} \end{aligned} \tag{12}$$

$$z^3(n) = \left(A_1(t)e^{i\omega_1 nT_s} + A_2(t)e^{i\omega_2 nT_s}\right)^3$$
$$= A_1^3(t)e^{i3\omega_1 nT_s} + A_2^3(t)e^{i3\omega_2 nT_s} + 3A_1^2(t)A_2(t)e^{i(2\omega_1+\omega_2)nT_s} + 3A_2^2(t)A_1(t)e^{i(\omega_1+2\omega_2)nT_s} \quad (13)$$

$$z^4(n) = \left(A_1(t)e^{i\omega_1 nT_s} + A_2(t)e^{i\omega_2 nT_s}\right)^4$$
$$= A_1^4(t)e^{i4\omega_1 nT_s} + A_2^4(t)e^{i4\omega_2 nT_s} + 4A_1^3(t)A_2(t)e^{i(3\omega_1+\omega_2)nT_s} + 4A_1^2(t)A_2^2(t)e^{i(2\omega_1+2\omega_2)nT_s} + 4A_2^3(t)A_1(t)e^{i(\omega_1+3\omega_2)nT_s} \quad (14)$$

C. SPECTRAL DISPLACEMENT OF HIGHER-ORDER COMPONENTS IN THE FUNDAMENTAL WAVEFORM SIGNAL

This section focuses on the lower-order harmonics generated by higher-order terms and explores methods for optimizing intermodulation components of sum and difference frequencies. As the higher-order term increases, so does the difference frequency component around the lower-order harmonic component. As depicted in Figure 6, there is a greater presence of differential frequency components surrounding the second harmonic of $x^6(n)$ compared to that of $x^4(n)$. Hence, it is insufficient to solely employ the complex harmonic polynomial of the fundamental signal z(n) for fitting the entire waveform. However, the second harmonic and fourth harmonic of $x^4(n)$ in the frequency spectrum exhibit equidistant sum and difference components, with the fundamental frequency interval serving as the fundamental unit.

By employing $z^4(n)$ and shifting its spectrum, we can effectively accommodate the second harmonic along with adjacent difference components as well as sum components of $x^4(n)$, wherein the shift distance on the frequency spectrum is measured in terms of units relative to the center frequency of the fundamental signal. Similarly, by performing two shifts on $z^6(n)$'s spectrum, we can respectively obtain the fourth harmonic, second harmonic, and associated sum and difference components of $x^6(n)$. After determining the calculation of the smallest unit f_c for spectrum shifting, it is essential to establish a precise methodology, and f_c is the central frequency of the fundamental wave. The frequencies of both the baseband signal and modulated signal are known, with f_0 representing the lowest frequency and f_1 denoting the highest frequency of the baseband signal. Additionally, f_{up} corresponds to the carrier signal's frequency. Formula (15) illustrates the calculation approach, wherein m signifies the number of leftward shifts.

$$f_{c,m} = -2m\left(\frac{(f_0+f_1)}{2} + f_{up}\right) \quad (15)$$

D. FWMP NONLINEAR MODEL

When m=1 is displaced by 1 unit, the digital sampling of $f_{c,1}$ becomes straightforward $f_{c,1}(n)$. To enhance clarity in

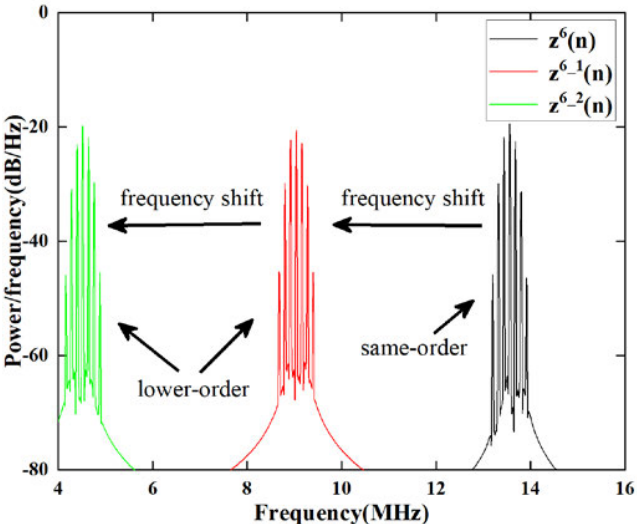

FIGURE 8. Fundamental complex signal spectrum shift.

expression, the frequency spectrum of the higher order term $z^k(n)$ is shifted by l units can denoted as $z^{k\_l}(n)$ as shown in formula (16). For instance, by shifting the spectrum of the fundamental complex signal $z^6(n)$ to the left once and twice, we obtain $z^{6\_1}(n)$ and $z^{6\_2}(n)$, respectively, as shown in Figure 8. The method of spectral shifting changes the position but not the shape of the spectrum for $z^6(n)$. In theory, lower-order components of higher-order terms in the fundamental wave can be obtained by performing spectral shifts on complexified higher-order terms. As higher-order terms require more spectral shifts, memory polynomial models with increasing parameters can further optimize model structure.

$$z^{k\_l}(n-q) = f_{c,l}(n)z^k(n-q) \quad (16)$$

To address the issue of reduced accuracy in nonlinear modeling of full-wave signals using conventional memory polynomials, we propose a decomposition approach that separates the fundamental signal, harmonics, and surrounding components such as sum and difference frequencies associated with the harmonics. Based on the previously discussed method of fitting the higher-order term into two parts separately, the higher-order term $x^k(n-q)$ of the memory polynomial can be sorted into formula (17), where L is the largest integer not exceeding $\frac{(K+1)}{2}$, and b_k is the lower-order harmonic coefficient of the higher-order term.

$$x^k(n-q) = z^k(n-q) + \sum_{l=1}^{L} b_k f_{c,l}(n)z^k(n-q) = z^k(n-q) + \sum_{l=1}^{L} b_k z^{k\_l}(n-q) \quad (17)$$

Subsequently, the fitted higher-order term $x^k(n-q)$ is incorporated into the memory polynomial equation (3), yielding the comprehensive FWMP model as depicted in equation (18). Herein, a_{kq} represents the coefficient of the

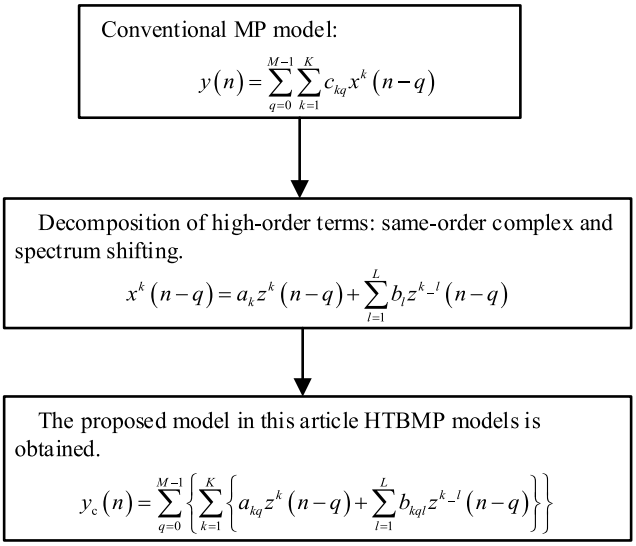

FIGURE 9. The FWMP-PA model proposed in this article.

corresponding order component within the higher-order term, while b_{kql} denotes the coefficient of its associated low-order component. The Hilbert transform of the PA output in the real number field gives $y_c(n)$.

$$y(n)=\sum_{q=0}^{M-1}\sum_{k=1}^{K}c_{kq}x^{k}(n-q)$$
$$y_{c}(n)=\sum_{q=0}^{M-1}\left\{\sum_{k=1}^{K}\left\{a_{kq}z^{k}(n-q)+\sum_{l=1}^{L}b_{kql}z^{k-l}(n-q)\right\}\right\} \tag{18}$$

Unlike conventional pre-distortion techniques, the utilized fundamental signal in this approach which is digitally modulated real domain signal and it is derived by complexified same-order plus frequency shifting, fundamental signal encompassing both the characteristics of the original baseband signal and those of the up-shifted signal. The scheme of proposed FWMP model shown as Figure 9.

E. PARAMETER EXTRACTION OF FWMP MODEL

As shown in Figure 2, in the stage of predistortion model extraction, the switch is set to position 1, and the initial value of the memory polynomial model is set to 1. This means that the fundamental signal u (n) is directly outputted from FWMP-DPD, and after negative feedback, we obtain the output signal x_d for the predistorter. When u (n) $-\lambda\tilde{y}_k$ (n) $\approx$ Ö0, which indicates that a linearized output will be obtained from the iteration format as equation (1), in this case x_k (n) is x_d; In order to determine the parameters of the FWMP model, we utilize the fundamental signal as input for the FWMP model and obtain x_d through feedback. Subsequently, we employ the least square method [15] to extract the parameters of this model. Once it achieves sufficient accuracy, it can be represented by formula (19), where U denotes the matrix representing the FWMP and a represents its parameter vector. Please refer to equation (21) for solving for the undetermined coefficient a.

$$x_d = \boldsymbol{U}\boldsymbol{a} \tag{19}$$

Among them, $U =$

$$\left[\begin{Bmatrix} z(1) & z(2) & \dots & z(m) \\ z(2) & z(3) & \dots & z(m+1) \\ \vdots & \vdots & \ddots & \vdots \\ z(n-m+1) & z(n-m+2) & \dots & z(n) \end{Bmatrix}\right.$$
$$\begin{Bmatrix} z^2(1) & z^2(2) & \dots & z^2(m) \\ z^2(2) & z^2(3) & \dots & z^2(m+1) \\ \vdots & \vdots & \ddots & \vdots \\ z^2(n-m+1) & z^2(n-m+2) & \dots & z^2(n) \end{Bmatrix}$$
$$\begin{Bmatrix} z^{2-1}(1) & z^{2-1}(2) & \dots & z^{2-1}(m) \\ z^{2-1}(2) & z^{2-1}(3) & \dots & z^{2-1}(m+1) \\ \vdots & \vdots & \ddots & \vdots \\ z^{2-1}(n-m+1) & z^{2-1}(n-m+2) & \dots & z^{2-1}(n) \end{Bmatrix}$$
$$\dots \begin{Bmatrix} z^{k}(1) & z^{k}(2) & \dots & z^{k}(m) \\ z^{k}(2) & z^{k}(3) & \dots & z^{k}(m+1) \\ \vdots & \vdots & \ddots & \vdots \\ z^{k}(n-m+1) & z^{k}(n-m+2) & \dots & z^{k}(n) \end{Bmatrix}$$
$$\begin{Bmatrix} z^{k-1}(1) & z^{k-1}(2) & \dots & z^{k-1}(m) \\ z^{k-1}(2) & z^{k-1}(3) & \dots & z^{k-1}(m+1) \\ \vdots & \vdots & \ddots & \vdots \\ z^{k-1}(n-m+1) & z^{k-1}(n-m+2) & \dots & z^{k-1}(n) \end{Bmatrix}$$
$$\left.\dots \begin{Bmatrix} z^{k-l}(1) & z^{k-l}(2) & \dots & z^{k-l}(m) \\ z^{k-l}(2) & z^{k-l}(3) & \dots & z^{k-l}(m+1) \\ \vdots & \vdots & \ddots & \vdots \\ z^{k-l}(n-m+1) & z^{k-l}(n-m+2) & \dots & z^{k-l}(n) \end{Bmatrix}\right] \tag{20}$$

$$a = \left(U^{H}U\right)^{-1}U^{H}x_d \tag{21}$$

III. ALGORITHM SIMULATION AND EXPERIMENTAL VERIFICATION OF FWMP PREDISTORTION MODEL

A. ALGORITHM SIMULATION

Firstly, the PA characteristics are simulated. The fundamental wave consists of dual-tone baseband signals which is 100KHz and 150KHz and the up-conversion signal frequency which is 2MHz. The fundamental wave is utilized in MATLAB. Considering the minimum sampling rate requirement of 125M for arbitrary function generators (Keysight M8190A), we have opted for a signal generation sampling rate of 126MHz. A fifth-order memory-free polynomial is assumed as the full-wave nonlinear model for the PA, with respective coefficients of 1, 0.1, 0.01, 0.001, and 0.0001. As depicted in Figure 10, simulation results demonstrate that the full wave comprises not only the fundamental wave component but also harmonics, their sum and difference components along with

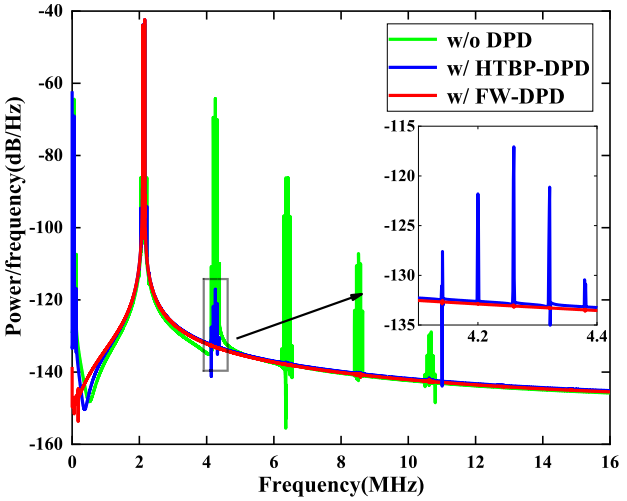

FIGURE 10. Comparison of predistortion performance between FWMP model and HTBP model.

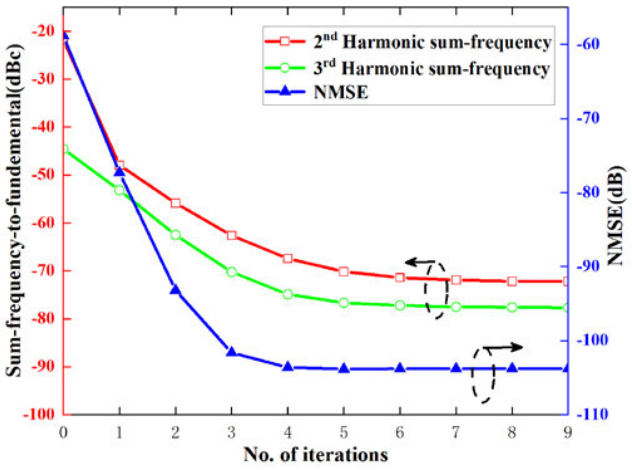

FIGURE 11. Iterative changes in the NMSE and sum-frequencies.

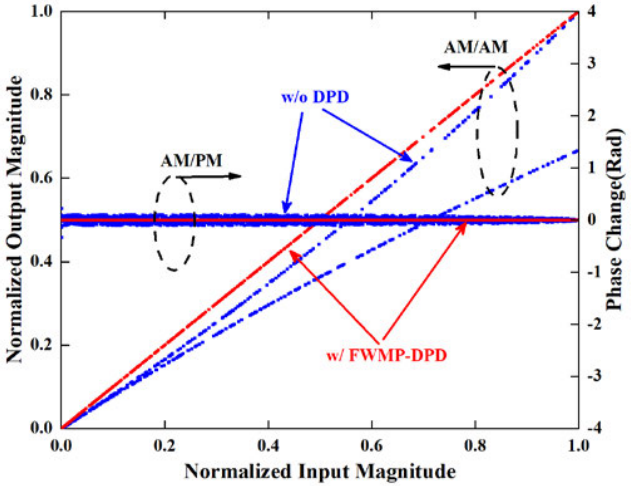

FIGURE 12. AM/AM and AM/PM curves for the fundamental dual-tone signals.

DC components; moreover, the sum of harmonics surpasses individual harmonic components while there exists a lower magnitude difference frequency component beyond harmonics range - consistent with theoretical analysis presented in Part II. Prior to implementing full wave predistortion technique, obtaining target output from predistorter necessitates employing negative feedback iteration method wherein negative feedback coefficient values $\lambda = 1.0$ and $w_0 = 0.6$ are used for nine iterations.

Subsequently, the HTBP model and the FWMP model are employed for parameter extraction of the predistorter. Subsequently, the original test two-tone signals undergo predistortion using HTBP-DPD and FWMP-DPD respectively before being transmitted to the PA model. The resultant full-wave signals from the PA reflect the linearization effect of predistortion. Figure 10 illustrates spectrum simulation results of PA output full-wave signals obtained through different predistortion models after linearization. The proposed FWMP-DPD model in this study exhibits superior suppression capabilities for harmonics, intermodulation, as well as sum and difference frequencies compared to HTBP-DPD model. Specifically, an improvement of approximately 15 dB is achieved for second-harmonic and sum-frequency components.

In each iteration, the input and output signals of the PA's model are updated, and Figure 11 illustrates the residual error of the harmonic-to-fundamental in the original input-output relationship of the PA. It is evident that negative feedback iterations exhibit rapid convergence, effectively mitigating second and third harmonics, thereby satisfying linearization requirements.

In addition, the AM/AM and AM/PM curves of the input-output signals of the FWMP-DPD scheme, as depicted in Figure 12. It is important to note that, for a more accurate representation of the phase information of the PA, both the complex values of the PA input signal and output signal be obtained by converting real into complex values. Without employing the HC-DPD scheme, distinct distortions between positive semicircles (where signal amplitude is positive) and negative semicircles (where signal amplitude is negative) can be clearly identified in different branches within the AM/AM curve. The proposed FWMP-DPD scheme significantly enhances system linearity, thereby eliminating the need for a filter bank as PA output satisfies linearization requirements.

B. TEST SETUP AND TEST RESULTS

In order to assess the linearization performance of the proposed FWMP model, a DPD shortwave test platform was constructed, as depicted in Figure 13. The input fundamental wave signal for the PA was generated using MATLAB, employing dual-tone signals with baseband frequencies of 100KHz and 150KHz as test signals, sampling rate of 126MHz, while carrier signals at digital up-conversion

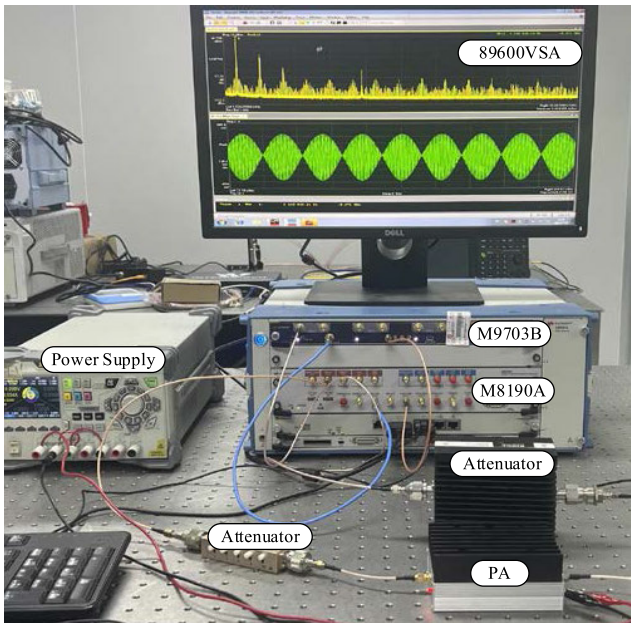

FIGURE 13. Full wave DPD experimental verification platform.

frequencies of 2, 6, 12, and 18MHz were utilized. The baseband signal, post digital modulation, is converted into an analog signal by employing an arbitrary waveform generator (Keysight M8190A) as the input for the PA. Subsequently, the amplified full-wave output undergoes a 40 dB attenuation before being captured using a digitizer (Keysight M9703B). Both the arbitrary waveform generator and digitizer operate on synchronized clocks, with the former serving as the trigger source for the latter. In this study, a high-frequency PA with an output power of 5 watts and a gain of 47 dB, fabricated using CMOS technology, was employed as the test amplifier. Spectrum analysis and data storage were performed using the Keysight 89600 Vector Signal Analysis software.

In order to comprehensively validate the suppression capability of the proposed FWMP towards harmonic and intermodulation components in the full-wave signal, separate modeling of the PA and predistorter is conducted. Initially, the output of the PA is collected, followed by employing various PA models such as MP model and HTBP model for characterization purposes, thereby comparing their respective nonlinear modeling capabilities.

The Normalized Mean Square Error (NMSE) was employed for assessing the efficacy of the modeling approach. The NMSE is computed using formula (22), where N represents the length of the test signal, y (n) denotes the actual output of the model, and $\tilde{y}(n)$ signifies the fitted value of the model's output.

$$NMSE = 10lg\left(\frac{\sum_N |y(n) - \tilde{y}(n)|^2}{\sum_N |y(n)|^2}\right) \tag{22}$$

The test results for PA modeling are presented in Table 1, wherein the NMSE of the MP model is approximately 8 dB higher compared to that of the HTBP model. Moreover, the FWMP model exhibits a 7 dB increase over the MP model and around a 15 dB increase over the HTBP model. In contrast to MP and HTBP models, FWMP demonstrates superior accuracy in simulating PA's time domain output characteristics. The predistorter output is obtained through negative feedback iteration method incorporating the PA model, while DPD model is constructed using FWMP. Table 1 and Table 2 the real framework length for DPD training is 504000.

TABLE 1. Comparison of fitting effect of different PA model's NMSE.

Model	2MHz	6MHz	12MHz	18MHz
HTBP (dB)	-60.1	-59.4	-58.8	-61.1
MP (dB)	-68.6	-68.2	-68.0	-70.2
FWMP (dB)	**-75.0**	**-75.5**	**-76.1**	**-77.1**

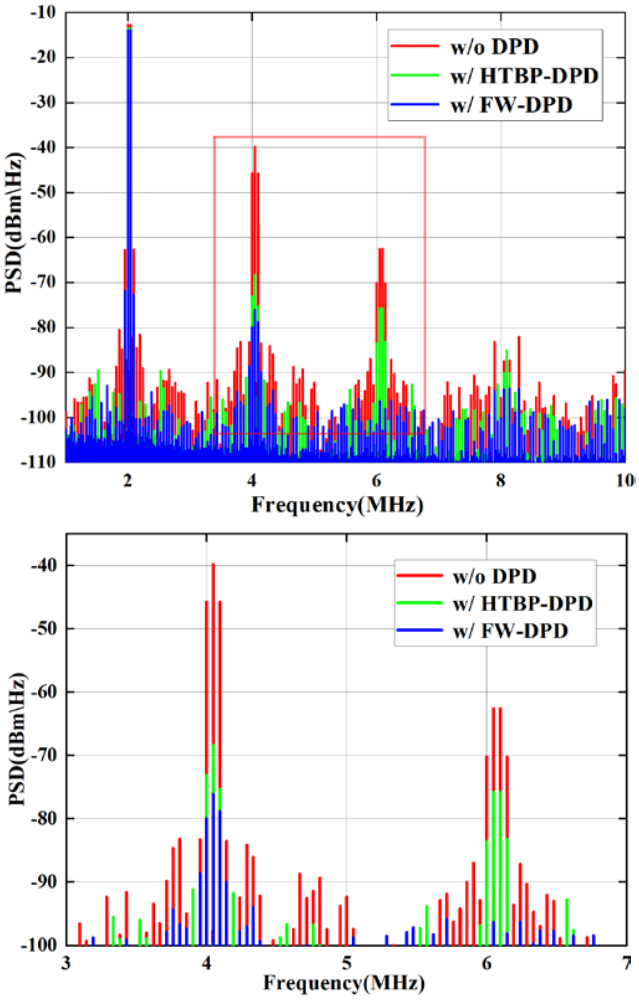

FIGURE 14. Predistortion performance comparison at 2MHz.

TABLE 2. linearization results of different DPD models.

Model\Frequency (MHz)		2	6	12	18
2nd Harmonic sum-frequency to fundamental (dBc)	NO-DPD	-26.6	-27.2	-28.9	-29.2
	HTBP	-55.8	-56.5	-57.4	-57.7
	FWMP	**-64.1**	**-65.8**	**-66.2**	**-67.8**
3rd Harmonic sum-frequency to fundamental (dBc)	NO-DPD	-49.2	-50.2	-50.7	-50.3
	HTBP	-62.6	-62.3	-63.1	-63.8
	FWMP	**-82.2**	**-82.0**	**-82.6**	**-82.6**

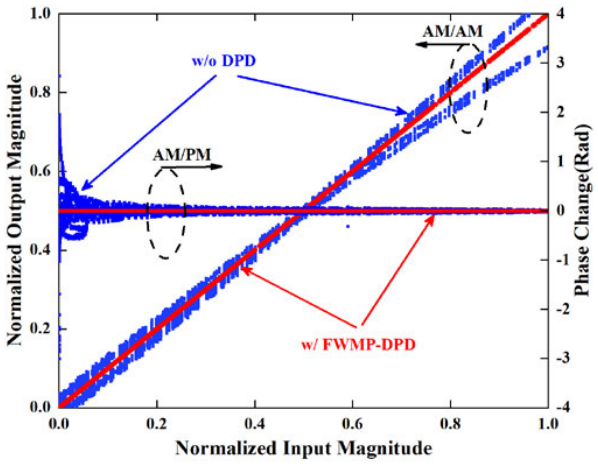

FIGURE 15. AM/AM and AM/PM curves for the fundamental dual-tone signals.

The original signal passes through digital predistorter and sent to the PA. Due to the sum-frequency component nearby second and third harmonics is the largest. For instance, in the case of a modulated signal which is fundamental wave comprising two frequencies, f_1 and f_2, the second harmonics would be $2f_1$ and $2f_2$ respectively. Apart from these second harmonics, there exists a sum-frequency component f_1+f_2, which exhibits the highest energy in proximity to the second harmonics as depicted in formula (12) and Figure 7. Similarly, the sum-frequency around the third harmonics is the largest. The statistics presented in Table 2 exclusively depict the sum-frequency components improve value of the second and third harmonics under different carriers. Based on the measured data, it is evident that the FWMP-DPD model outperforms the HTBP model. In comparison to HTBP, a minimum improvement of 35 dB can be achieved for harmonics, along with an approximate enhancement of 8 dB for intermodulation. Figure 14 illustrates a typical predistortion effect, which aligns with formulas (12)-(14) discussed in Section II and simulation results obtained from our algorithm. The signal output from the PA exhibits a higher sum-frequency component compared to the second harmonic itself, and a higher sum-frequency component compared to the third harmonic.

Figure 15 illustrates the verification results of the AM/AM and AM/PM characteristics of the actual PA. Similar to the simulation presented in Figure 12, these data points represent complex values obtained by converting the real-domain input and output signals of the PA. The dispersion observed in these curves indicates a certain memory effect present in the PA. However, after FWMP-DPD processing, a noticeable enhancement in linearity is achieved, as evidenced by improved convergence between AM/AM and AM/PM characteristics, consistent with algorithm simulation outcomes.

Following DPD linearization, significant improvements are observed in both the harmonic components and their respective sum and difference frequency components. Notably, there is a remarkable enhancement of 34 dB for the second harmonics and 36 dB for the sum-frequency component.

IV. CONCLUSION

This article presents a novel full-wave DPD model, which revolutionizes the conventional memory polynomial model employed for baseband DPD by effectively mitigating both intermodulation and harmonic distortion in PA. The comprehensive mathematical derivation of the proposed full-wave DPD is provided, verification. The distinctive aspect of this study lies in utilizing the fundamental wave signal that is modulated signals, constructing harmonic signals through complexification of the fundamental wave polynomial, as well as introducing methods for complexification of the fundamental wave signal and frequency spectrum shifting. Simulation results along with experimental validation demonstrate the remarkable efficacy of the proposed full-wave predistortion model in suppressing intermodulation and harmonic distortion in shortwave PA.

REFERENCES

[1] D. R. Morgan, Z. Ma, J. Kim, M. G. Zierdt, and J. Pastalan, "A generalized memory polynomial model for digital predistortion of RF power amplifiers," *IEEE Trans. Signal Process.*, vol. 54, no. 10, pp. 3852–3860, Oct. 2006, doi: 10.1109/TSP.2006.879264.

[2] A. E. Abdelrahman, O. Hammi, A. K. Kwan, A. Zerguine, and F. M. Ghannouchi, "A novel weighted memory polynomial for behavioral modeling and digital predistortion of nonlinear wireless transmitters," *IEEE Trans. Ind. Electron.*, vol. 63, no. 3, pp. 1745–1753, Mar. 2016, doi: 10.1109/TIE.2015.2494040.

[3] A. Abdelhafiz, L. Behjat, and F. M. Ghannouchi, "Generalized memory polynomial model dimension selection using particle swarm optimization," *IEEE Microw. Wireless Compon. Lett.*, vol. 28, no. 2, pp. 96–98, Feb. 2018, doi: 10.1109/LMWC.2017.2783847.
[4] G. Xu, T. Liu, and Y. Ye, "Linearization of HF power amplifiers with digital predistortion techniques," in *Proc. Int. Conf. Electron., Commun. Control (ICECC)*, Ningbo, China, Sep. 2011, pp. 2706–2708, doi: 10.1109/ICECC.2011.6066497.
[5] X. Liu, W. Chen, L. Chen, and Z. Feng, "A robust and broadband digital predistortion utilizing negative feedback iteration," in *IEEE MTT-S Int. Microw. Symp. Dig.*, Chengdu, China, May 2018, pp. 1–4, doi: 10.1109/IEEE-IWS.2018.8400950.
[6] I. Kashchenko, "The harmonic injection technique for short-wave HF power amplifier," in *Proc. Dyn. Syst., Mech. Mach. (Dynamics)*, Omsk, Russia, Nov. 2017, pp. 1–6, doi: 10.1109/Dynamics.2017.8239460.
[7] P. Pazhouhesh and J. Kitchen, "A broadband class AB power amplifier with second harmonic injection," in *Proc. IEEE 14th Dallas Circuits Syst. Conf. (DCAS)*, Dallas, TX, USA, Nov. 2020, pp. 1–5, doi: 10.1109/DCAS51144.2020.9330364.
[8] S. Wang, M. Roger, J. Sarrazin, and C. Lelandais-Perrault, "An efficient method to study the tradeoff between power amplifier efficiency and digital predistortion complexity," *IEEE Microw. Wireless Compon. Lett.*, vol. 29, no. 11, pp. 741–744, Nov. 2019, doi: 10.1109/LMWC.2019.2939911.
[9] H. K. Singhal and K. Rawat, "Digitally assisted harmonic cancellation for multi-octave filter-less transmitter," *IEEE Access*, vol. 8, pp. 68913–68929, 2020, doi: 10.1109/ACCESS.2020.2986264.
[10] K.-J. Cho, D.-H. Jang, S.-H. Kim, J.-H. Kim, B. Lee, N.-Y. Kim, J.-C. Lee, and S. P. Stapleton, "Multi-order predistortion of power amplifiers using a second harmonic based technique," *IEEE Microw. Wireless Compon. Lett.*, vol. 13, no. 10, pp. 452–454, Oct. 2003, doi: 10.1109/LMWC.2003.815186.
[11] L. Chen, W. Chen, Y.-J. Liu, X. Chen, F. M. Ghannouchi, and Z. Feng, "A robust and scalable harmonic cancellation digital predistortion technique for HF transmitters," *IEEE Trans. Microw. Theory Techn.*, vol. 68, no. 7, pp. 2796–2807, Jul. 2020, doi: 10.1109/TMTT.2020.2979438.
[12] G. Xu, T. Liu, Y. Ye, and X. Zhang, "Hybrid harmonic-intermodulation distortion behavioral model for shortwave power amplifiers," *Int. J. RF Microw. Comput. Aided Eng.*, vol. 29, no. 7, 2019, Art. no. e21718.
[13] J. Ren, X. Wang, and Q. Cheng, "An integrated cancelling method of harmonic and intermodulation distortion of short-wave power amplifier based on digital predistortion," *IEEE Microw. Wireless Compon. Lett.*, vol. 32, no. 10, pp. 1223–1226, Oct. 2022, doi: 10.1109/LMWC.2022.3174045.
[14] Z. Liu, Z. Chen, and C. Zhao, "An HC-DVR model for harmonic-cancellation digital predistortion," in *Proc. IEEE 22nd Int. Conf. Commun. Technol. (ICCT)*, Nanjing, China, Nov. 2022, pp. 318–321, doi: 10.1109/ICCT56141.2022.10073157.
[15] L. Guan and A. Zhu, "Optimized low-complexity implementation of least squares based model extraction for digital predistortion of RF power amplifiers," *IEEE Trans. Microw. Theory Techn.*, vol. 60, no. 3, pp. 594–603, Mar. 2012, doi: 10.1109/TMTT.2011.2182656.
[16] O. Hammi and F. M. Ghannouchi, "Power alignment of digital predistorters for power amplifiers linearity optimization," *IEEE Trans. Broadcast.*, vol. 55, no. 1, pp. 109–114, Mar. 2009, doi: 10.1109/TBC.2008.2006652.
[17] S. Wang, M. A. Hussein, O. Venard, and G. Baudoin, "Impact of the normalization gain of digital predistortion on linearization performance and power added efficiency of the linearized power amplifier," in *Proc. 12th Eur. Microw. Integr. Circuits Conf. (EuMIC)*, Nuremberg, Germany, Oct. 2017, pp. 310–313, doi: 10.23919/EuMIC.2017.8230720.

JUNSHI LV (Student Member, IEEE) received the B.S. degree in electrical and automation engineering from Sanjiang University, Nanjing, China, in 2014, and the M.S. degree from the Faculty of Electrical Engineering and Computer Science, Ningbo University (NBU), Ningbo, China, in 2020, where he is currently pursuing the Ph.D. degree.

His research interests include wireless communications, with a focus on high-efficiency radio frequency (RF) power amplifiers (PA) design, analog and digital predistortion (DPD), and nonlinear modeling.

GAOMING XU received the B.S. degree in electronic and information engineering from the Naval Aeronautical Engineering Academy, Qingdao, China, in 2007, and the M.S. and Ph.D. degrees from the Faculty of Electrical Engineering and Computer Science, Ningbo University (NBU), Ningbo, China, in 2010 and 2015, respectively. He is currently an Associate Professor with the Faculty of Electrical Engineering and Computer Science, NBU. His research interests include wireless communications, with a focus on high-efficiency RF power amplifier design, digital predistortion, analog predistortion, and nonlinear modeling.

CHENGTING ZHANG received the degree in communication engineering from the South China University of Technology, in 2008, and the master's degree in network engineering from Zhejiang University, in 2010. He is currently a Senior Engineer of network administration with China Tobacco Zhejiang Industrial Company Ltd. His research interests include computer communication technology and network security.

HAILI ZHANG received the B.S. degree from Henan University, in 2003, and the M.S. degree in material engineering from the University of Electronic Science and Technology of China, in 2008. He is currently pursuing the Ph.D. degree with Ningbo University. As a Research and Development Manager, he was with Dongguan ACE Technology Company Ltd., Guangdong Shenglu Telecommunication Technology Company Ltd., and Shenzhen Dafu Telecommunication Technology Company Ltd., from 2006 to 2009. In 2010, he joined the Zhejiang Fashion Institute of Technology, where he established the Department of Urban Rail Communication, involving management, teaching, and research. His research interests include RF modules and high-isolation antennas.

TAIJUN LIU (Senior Member, IEEE) received the B.S. degree in applied physics from China University of Petroleum, Dongying, China, in 1986, the M.Eng. degree in electrical engineering from the University of Electronic Science and Technology of China, Chengdu, China, in 1989, and the Ph.D. degree from École Poly Technique de Montréal, Université de Montréal, Montreal, QC, Canada, in 2006. He is currently with the Faculty of Electrical Engineering and Computer Science, Ningbo University, as a Professor. His current research interests include nonlinear modeling and linearization for wideband transmitters/power amplifiers, the Intelligent IoT, intelligent wireless sensing, and ultra-linear high-efficiency intelligent power amplifiers for broadband wireless and satellite communications systems.